# Non-Reciprocal Balanced Bandpass Filters with Quasi-Elliptic Response

Dakotah Simpson, *Member, IEEE*, Photos Vryonides, *Senior Member, IEEE*, Symeon Nikolaou, *Member, IEEE*, and Dimitra Psychogiou, *Senior Member, IEEE*

***Abstract*—This paper reports on the RF design and practical development of a non-reciprocal balanced bandpass filter (BPF) that exhibits a highly-selective quasi-elliptic response in the forward direction of propagation that is shaped by four transmission poles and two transmission zeros (TZs). By modulating some of the filter's resonators with phase-progressed AC signals, a non-reciprocal response is obtained in the differential mode. Its common-mode is also highly suppressed due to the incorporation of a balanced network that results in two additional TZs and resistive loss that are unique to the common-mode. The filter order can be increased by cascading additional resonators. For validation purposes, a microstrip prototype centered at 725 MHz was designed, manufactured, and measured. It showed a high isolation in the differential-mode reverse transmission of up to 62.1 dB. Moreover, the common-mode was suppressed by over 45 dB in a bandwidth greater than one octave.**

***Index Terms*—Balanced filter, bandpass filter, isolator, microstrip filter, non-reciprocal filter, non-reciprocity.**

## I. Introduction

BALANCED RF bandpass filters (BPFs) and other balanced devices are a popular topic of research due to their advantages of higher immunity to certain types of electromagnetic interference over their single-ended counterparts [1]-[9]. As such, a large variety of balanced BPFs have been presented to date in both planar and 3D configurations using multi-mode resonators. The majority of them are based on incorporating two identical single-ended filters within a balanced network that is appropriately designed to reject the common-mode signals. Nevertheless, the reported balanced BPFs exhibit low-order transfer functions (2nd-order in [2] and [4]), high levels of insertion loss (IL) (up to 6.8 dB in [3] and 3.9 dB in [4]), or low levels of in-band common-mode suppression (9.3 dB in [2] and ~20 dB in [5] and [6]).

Other research efforts are focusing on developing filtering devices with non-reciprocal transfer functions to miniaturize RF front-ends and protect them from high-power reflected signals or separate their transmit and receive channels [10]-[14]. Miniaturization is targeted by incorporating the functionalities of a BPF and an isolator within a single device, alleviating the need for two separate components. Miniaturization is further enhanced by using magnetless design approaches such as spatio-temporal modulation (STM) to achieve non-reciprocity [10]-[14]. Specifically, STM breaks the time-reversal symmetry through the modulation of the

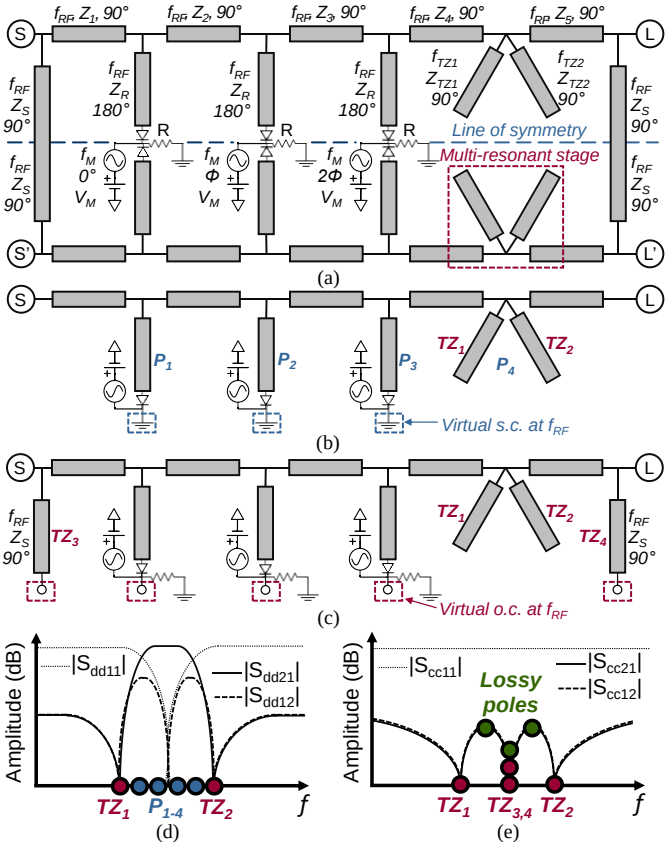


**Fig. 1.** Non-reciprocal balanced BPF with quasi-elliptic power transmission response. (a) Overall schematic. (b) Single-ended equivalent schematic of the differential mode. (c) Single-ended equivalent schematic of the common mode. (d) Conceptual transfer function of the differential mode. (e) Conceptual transfer function of the common mode.

Manuscript received May 6, 2022. This work has been supported by NSF project No. ECCS-1941315. Aspects of this work have been in part supported by SFI project No. 20/RP/8334. *(Corresponding author: D. Simpson).*

D. Simpson is with the Department of Electrical, Computer, and Energy Engineering, University of Colorado Boulder, Boulder, CO 80309, USA (e-mail: dakotah.simpson@colorado.edu).

P. Vryonides and S. Nikolaou are with Frederick Research Center and Frederick University, Nicosia, 1036, Cyprus. (e-mails: p.vryonides@frederick.ac.cy and s.nikolaou@frederick.ac.cy).

D. Psychogiou is with University College Cork, Cork 021, T12 K8AF, Ireland and Tyndall National Institute, Cork, T12 R5CP, Ireland (e-mail: dpsychogiou@ucc.ie).

Color versions of one or more of the figures in this article are available online at http://ieeexplore.ieee.org

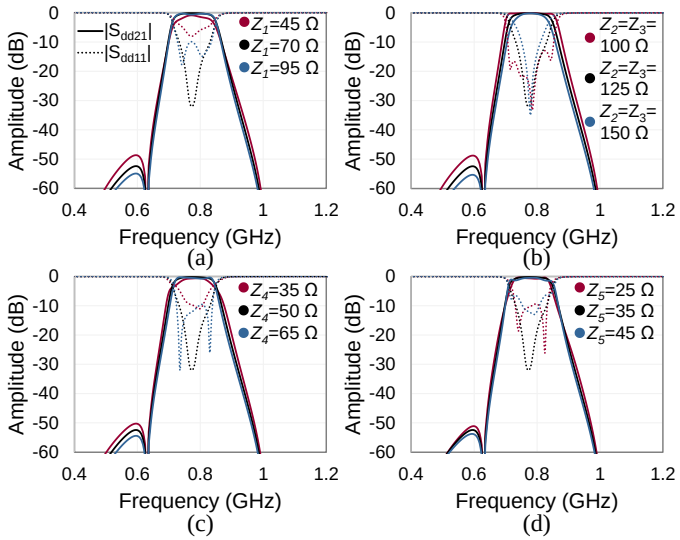


**Fig. 2.** Simulated differential-mode responses showing variation of the coupling impedance values. (a) Variation of $Z_1$. (b) Variation of $Z_2$ and $Z_3$. (c) Variation of $Z_4$. (d) Variation of $Z_5$. Values for parameters not being varied: $f_{RF}$ = 780 MHz, $f_{TZ1}$ = 630 MHz, $f_{TZ2}$ = 1010 MHz, $Z_{TZ1}$ = 60Ω, $Z_{TZ2}$ = 60Ω, $Z_1$ = 70Ω, $Z_2$=$Z_3$=125Ω, $Z_4$= 49Ω, $Z_5$ = 35Ω, $Z_R$ = 25Ω, and $Z_S$ = 50Ω. A realistic varactor from Skyworks SMV1413 is used.

resonators' resonant frequencies in time with low frequency AC signals and in space by introducing a phase progression between the BPF's resonators. Such design approaches have been successfully demonstrated for static [10], [11] and tunable [12]-[14] single-ended BPF designs utilizing lumped element [11]-[13] or microstrip [10], [14] integration schemes. Despite the widespread use of STM, it has not been used for the realization of balanced filter designs to date.

This manuscript investigates for the first time the potential to realize balanced BPFs by applying STM to some of the BPF resonators in order to obtain highly-selective non-reciprocal transfer functions in the differential mode and high levels of RF signal suppression in the common mode. Specifically, this paper examines a new class of a balanced BPF that exhibits a quasi-elliptic transmission response in its differential mode that is shaped by four transmission poles and two transmission zeros (TZs). A balanced network shaped by stubs and resistively terminated resonators is proposed to highly-suppress the common mode while not affecting the differential mode.

The rest of this paper is arranged as follows. Section II presents the theoretical background and design principles of the balanced BPF. In Section III, a microstrip prototype is demonstrated for practical validation. Lastly, Section IV reports a brief summary of the main contributions of this work.

## II. Theoretical Background

The circuit schematic and conceptual differential- and common-mode power responses of the proposed non-reciprocal BPF are shown in Fig. 1. In particular, Fig. 1(a) depicts the circuit schematic of the overall balanced BPF architecture and Figs. 1(b) and 1(c) show its single-ended equivalents under differential- and common-mode excitation, respectively. The

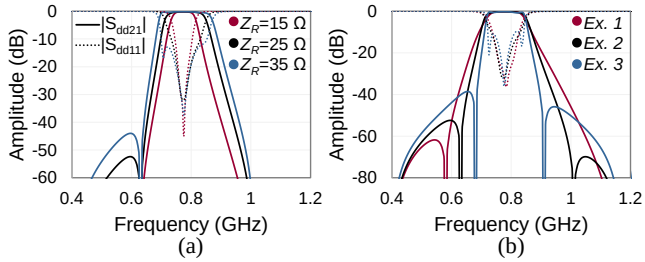


**Fig. 3.** Simulated differential-mode showing variation of the resonator parameters. (a) Variation of $Z_R$. (b) Variation of TZ location. Ex. 1: $f_{TZ1}$ = 580 MHz, $f_{TZ2}$ = 1170 MHz. Ex. 2: $f_{TZ1}$ = 630 MHz, $f_{TZ2}$ = 1010 MHz. Ex. 3: $f_{TZ1}$ = 680 MHz, $f_{TZ2}$ = 910 MHz. The rest of the component values are listed in Fig. 2.

balanced filter's two RF input and output ports are connected through two quarter-wavelength-long lines (i.e., impedance inverters) with an impedance $Z_S$. RF energy is coupled from the input to the output ports through an alternating cascade of impedance inverters, resonators, and a multi-resonant stage that are mirrored across the line of symmetry. Specifically, there are three half-wavelength-long open-circuit stubs, each introducing one transmission pole at the passband, and one multi-resonant stage, which comprises two open-circuit quarter-wavelength-long stubs and adds one pole and two TZs to the response [3], [15]. The TZs are located at the resonant frequencies of the two stubs and the pole is located at the frequency where their two input impedances mutually cancel each other out. To achieve non-reciprocity, the STM is applied to the three half-wavelength resonators. These resonators are capacitively-loaded with reverse-biased varactor diodes and subsequently connected to their mirrored counterparts at the line of symmetry. Moreover, the resonators are also resistively-loaded at the line of symmetry with the purpose of suppressing the common mode as it will be explained later on.

### *A. Differential-Mode Excitation and Design*

Fig. 1(b) shows the single-ended equivalent circuit under differential-mode excitation. In this case, the line of symmetry acts as a virtual short circuit. Thus, the lines connecting the RF input and output ports are shorted at the end of a quarter-wavelength-long line, resulting in an equivalent open circuit. They can therefore be neglected. The resistors can also be ignored since they are shorted. This results in a bandpass response with four poles (three from the open circuited stubs and one from the multi-resonant stage) and two TZs, as shown with $|S_{dd21}|$ in Fig. 1(d).

The bandpass response is designed through the tuning of the impedances and the locations of the TZs while the STM is off. Fig. 2 shows how the differential-mode response varies as the impedances of the coupling TLs are tuned. Specifically, it demonstrates that $Z_1$ and $Z_4$ mainly affect the passband shape and the return loss. $Z_5$ alters the near-band selectivity and return loss, while tuning $Z_2$ and $Z_3$ simultaneously changes the BW of the passband. Fig. 3 depicts how tuning the resonator characteristics can change the response. Fig. 3(a) shows that the BW of the response can be increased by increasing the impedance of the pole resonators, $Z_R$. Fig. 3(b) illustrates that varying the locations of the TZs changes the out-of-band

This article has been accepted for publication in IEEE Transactions on Circuits and Systems--II: Express Briefs. This is the author's version which has not been fully edited and content may change prior to final publication. Citation information: DOI 10.1109/TCSII.2022.3202860



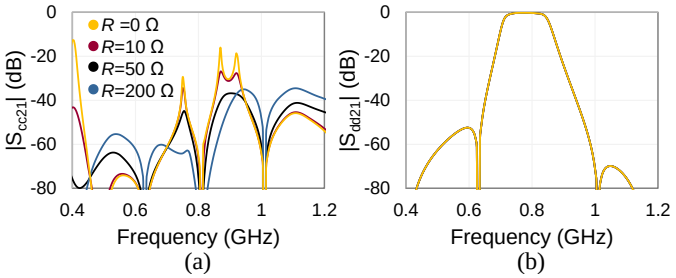


**Fig. 4.** Simulated transmission responses for different resistor values. (a) Common-mode. (b) Differential-mode. The rest of the component values are listed in the caption of Fig. 2.

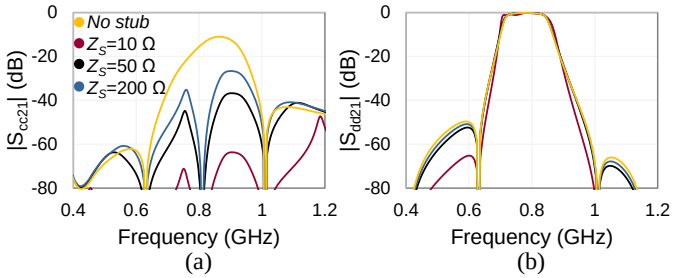


**Fig. 5.** Simulated transmission responses for different stub impedance values, $Z_S$. (a) Common-mode. (b) Differential-mode. The rest of the component values are listed in the caption of Fig. 2 with the addition of $R$ = 50 Ω.

response. This is achieved by changing the values of the $f_{TZ1}$ and $f_{TZ2}$, which determine the location of the TZs. Later, a non-reciprocal response is obtained by properly biasing the varactor diodes with progressively phased low frequency RF signals.

### *B. Common-Mode Excitation and Design*

Under the common-mode feeding condition, the line of symmetry can be replaced with an open circuit, leading to the single-ended circuit in Fig. 1(c). The open circuit permits the presence of the resistors, which introduce loss to the resonators and weaken the response of their resulting poles. Additionally, the lines at the inputs and outputs are now loaded with open circuited stubs that introduce two TZs that are only present in the common mode. They are located at the center frequency of the passband and further suppress the common-mode signals. The resulting common-mode response is shown in Fig. 1(e).

To demonstrate the impact of the resistors, Fig. 4 shows how the common- and differential-mode responses change as the value of R is varied while STM is off. If R is too low then the poles are not sufficiently loaded and result in peaks in the response. For large R-values the minimum in-band suppression and the out-of-band suppression decrease. Fig. 4(b) shows that the resistors have no effect on the differential-mode response.

Fig. 5 demonstrates the influence of the stubs at the input and output ports on the common- and differential-mode responses. Specifically, Fig. 5(a) shows that without the stubs and their resulting TZs, the common-mode response would only be suppressed by 11 dB. It also indicates that higher characteristic-impedances lead to less suppression. Therefore, it is beneficial to use the lowest impedance stubs that are practical. Fig. 5(b) reveals that the stubs increase the selectivity of the differential-mode response, but their effect is marginal.

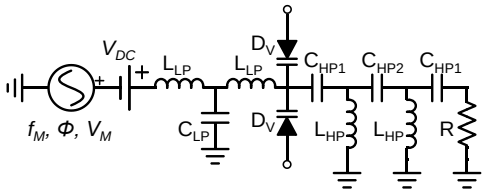


**Fig. 6.** Circuit-schematic of the DC and AC biasing networks. The resistors located at the line of symmetry are also included.

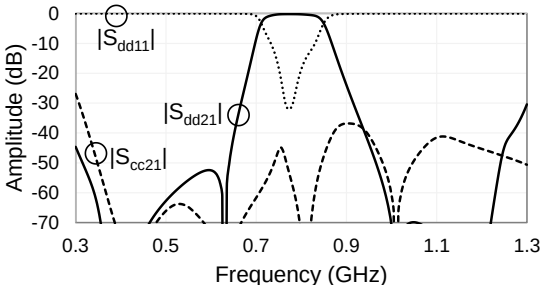


**Fig. 7.** Simulated S-parameters of the balanced BPF in Fig. 1 without modulation. The component values are listed in the caption of Fig. 2 with the addition of $R$ = 50 Ω, $V_{DC}$ = 4V, $L_{LP}$ = 140 nH, $C_{LP}$ = 56 pF, $C_{HP1}$ = 12 pF, $C_{HP2}$ = 6.8 pF, $L_{HP}$ = 22 nH, and $D_V$ is a lossy Skyworks SMV1413 varactor.

### *C. Bias Network Design*

The biasing of the varactor diodes determines their capacitance and consequently the resonant frequencies of the resonators that they are loading. They are biased with both DC and AC signals. The DC biasing sets the average capacitance value and the time-dependent AC biasing modulates the capacitance in time. A detailed schematic of the biasing circuit at the line of symmetry is shown in Fig. 6. A lowpass filter (LPF) with components $L_{LP}$ and $C_{LP}$ is used to reject RF signals from reaching the AC and DC sources. In order to keep the biasing signals from leaking into the loading resistors (placed to suppress the common mode) and causing unnecessary power losses, a highpass filter (HPF) with a cut-off frequency higher than $f_M$ precedes the resistor. The HPF allows the RF signals to reach the resistor while presenting high impedances to the AC and to DC sources. Grounded LPFs are added at the input of the second resonators to ground the anodes of all varactor diodes.

### *D. Non-Reciprocal Filter Design Method*

An example simulated response of a non-modulated filter is shown in Fig. 7 for a center frequency of 780 MHz and a BW of 130 MHz (16.7%). As it can be seen, the differential-mode response is selective due to comprising four poles and two TZs, while the common-mode response is highly suppressed due to the presence of the TZs and the resistive resonator loading.

For STM to work, a progressive phase shift needs to be applied to the AC signals from the varactor nearest the input of the filter to the one nearest the output. The transfer-function-determining characteristics of the AC signals are their frequency ($f_M$, where $f_M << f_{RF}$), phase progression ($\Phi$), and amplitude ($V_M$). The parameters are determined by performing parametric sweeps. The goal is to obtain high isolation (IS, >20 dB) in the reverse transmission direction ($|S_{dd12}|$), while maintaining a low IL (<4 dB) in the forward direction ($|S_{dd21}|$).

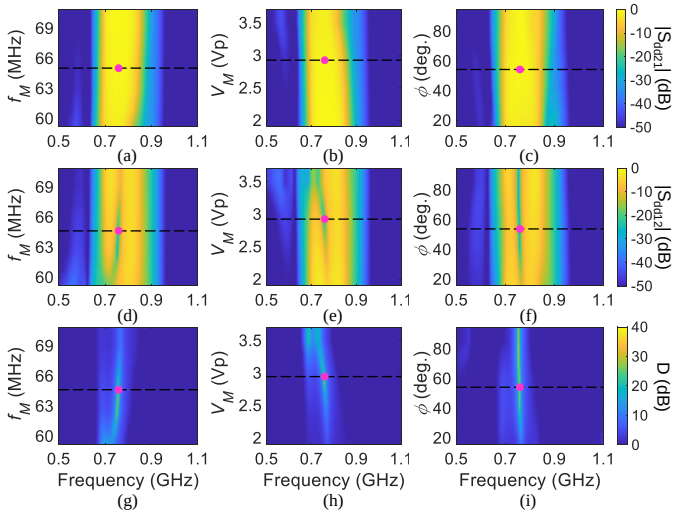


**Fig. 8.** Simulated S-parameters of the filter in Fig. 1 when the STM is present and the modulation parameters are swept. The component values are listed in Fig. 7. The pink colored dots indicate the optimal values at $f_{cen}$. (a) $|S_{dd21}|$ as $f_M$ is varied. (b) $|S_{dd21}|$ as $V_M$ is varied. (c) $|S_{dd21}|$ as $\Phi$ is varied. (d) $|S_{dd12}|$ as $f_M$ is varied. (e) $|S_{dd12}|$ as $V_M$ is varied. (f) $|S_{dd12}|$ as $\Phi$ is varied. (g) D as $f_M$ is varied. (h) D as $V_M$ is varied. (i) D as $\Phi$ is varied.

The S-parameters of the balanced BPF in Fig. 7 under STM modulation are shown in Fig. 8. $D$ is the directivity and is calculated as the difference between the forward, $|S_{dd21}|$, and backward transmissions, $|S_{dd12}|$. The optimal values of each parameter have been marked with a dashed line in each plot, whereas $f_{cen}$ is marked with a pink colored dot. The parameters were found through an iterative process. It is observed that when $f_M$ is approximately equal to BW/2, optimum non-reciprocal performance is obtained (also mentioned in [12], [13] for single-ended BPFs). This is the starting point for $f_M$. The other parameters were first simulated over wide ranges with large step sizes. The range and step size were continually decreased as the ideal parameter values were narrowed down.

The first column of Fig. 8 shows how the response changes as the $f_M$ is varied. When $f_M$ is too low, the IL increases while the IS decreases. On the other hand, a high $f_M$ results in poor IS. For the designed filter, an $f_M$ of 65 MHz provides high IS and low IL. The second column of Fig. 8 depicts the responses of the filter when $V_M$ is swept. When the voltage is set too low or too high, the IS decreases. The optimum $V_M$ is 2.95 V for this filter. The third column shows how the response reacts to a change in $\Phi$. As shown, this parameter has less of an effect than the others. When it is too low or too high, the IS suffers.

### *E. Extension to Higher-Order Designs*

The schematic in Fig. 9 shows that the four-pole/two-TZ BPF can be extended to higher-order transfer functions by cascading additional resonators and multi-resonant stages at the accesses of the filter. Fig. 9 demonstrates this for a six-pole/four-TZ BPF. The newly added pole resonator can either be modulated or non-modulated. Fig. 10 compares the responses of the filter in Fig. 9 when 3 or four resonators are modulated. Modulating the new resonator results in increased in-band isolation

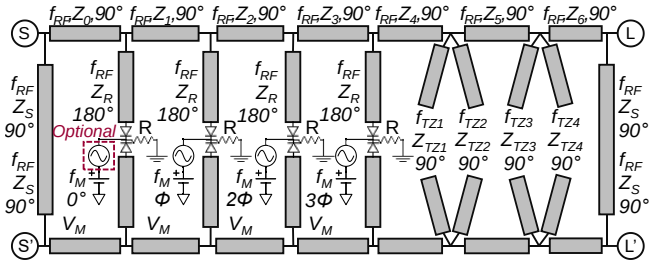


**Fig. 9.** Schematic showing the extension of the non-reciprocal balanced BPF in Fig. 1 to a six-pole/four-TZ filter.

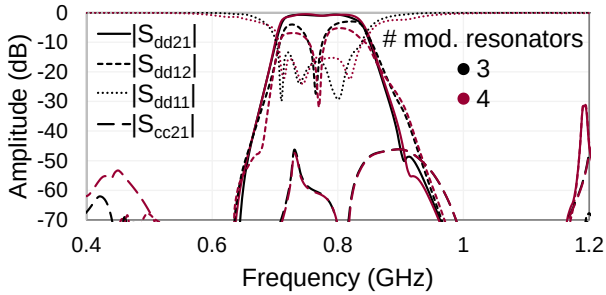


**Fig. 10.** Comparison of simulated modulated responses of the circuit in Fig. 9 when the first resonator is either modulated or non-modulated. The component values are: $f_{RF}$=780 MHz, $f_{TZ1}$= 630 MHz, $f_{TZ2}$=1010 MHz, $f_{TZ3}$=590 MHz, $f_{TZ4}$=1140 MHz, $Z_{TZ1}$ =$Z_{TZ2}$=60Ω, $Z_{TZ3}$=$Z_{TZ4}$=30Ω, $Z_1$=75Ω, $Z_2$=120Ω, $Z_3$=130Ω, $Z_4$= 69Ω, $Z_5$=30Ω, $Z_6$=35Ω, $Z_R$ = 25Ω, and $Z_S$ = 50Ω. 3 modulated resonators: $f_M$ = 65 MHz, $V_M$ = 2.73 $V_P$, and $\Phi$ = 54°. 4 modulated resonators: $f_M$ = 70 MHz, $V_M$ = 3.34 $V_P$, and $\Phi$ = 35°.

especially outside of the center frequency. However, adding isolation increases the complexity of the device since it requires more modulation signals.

## III. Experimental Validation

To validate the non-reciprocal balanced BPF concept, a microstrip prototype was designed, manufactured, and measured for $f_{cen}$ 740 MHz and a modulated-response BW of 100 MHz (13.5%). Its design follows the design steps in Section II. A photograph of the prototype is presented in Fig. 11. It was built on a 1.52-mm-thick Rogers RO4003C substrate. Skyworks SMV1413 varactor diodes were utilized as the tuning elements [16]. To provide the required biasing signals, three clock-synced arbitrary waveform generators were used. Its RF responses were measured with a four-port Keysight N5224A PNA. As identified in Fig. 11, two LPFs are utilised at the input of the second resonators in order to provide a ground for the DC and AC frequencies on the anode side of the varactor diodes.

In Fig. 12, a comparison of the EM-simulated and the RF-measured responses is shown. The measured $f_{cen}$ and BW of the modulated response are 725 MHz and 90 MHz, respectively. The minimum in-band IL in the forward direction is measured to be 3.2 dB, while the maximum IS in the reverse direction is 62.1 dB. The selective differential-mode response and highly-rejected common-mode response are maintained after including modulation. The common mode is rejected by 45 dB from 375 MHz to 1030 MHz (2.74:1) and at a maximum of 62 dB within the band. The filter of this work is compared to other non-

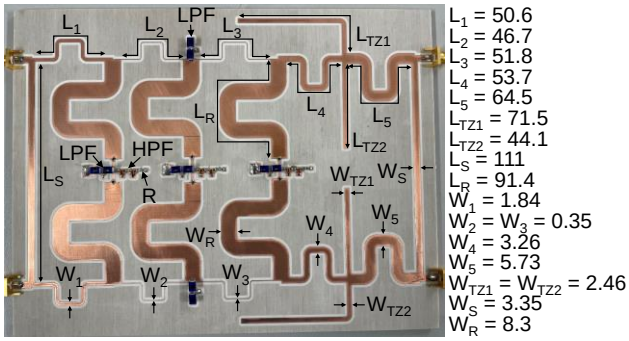


**Fig. 11.** Photograph of the non-reciprocal quasi-elliptic balanced BPF. Dimensions are in mm.

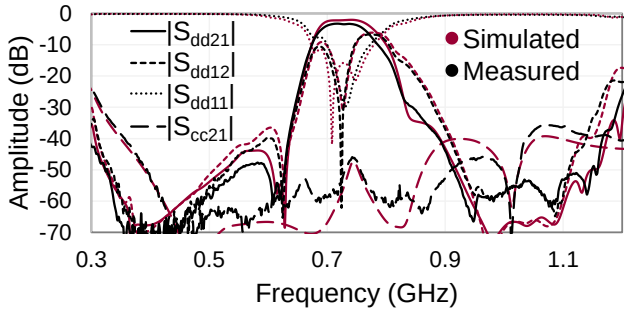


**Fig. 12.** Comparison of the EM-simulated and RF-measured responses of the prototype in Fig. 11.

TABLE I

COMPARISON WITH STATE-OF-ART NON-RECIPROCAL BPFS

| Work | $f_{cen}$, MHz | BW, MHz (%) | IL, dB | IS, dB | *N* | Bal. |
|---|---|---|---|---|---|---|
| **[10]** | 1020 | 65 (6.4) | 5.5 | 10-11.7 | 2 | N |
| **[11]** | 186 | 33 (17.7) | 1.5 | 8-23 | 3 | N |
| **[12]** | 136-163 | 27.5 (19.2) | 3.7 | 9-52.8 | 3 | N |
| **[13]** | 270-310 | 15-41.5 (5.2-14.3) | 1.7-4.3 | 6.5-30.9 | 3 | N |
| **[14]** | 885-1031 | 42 (4.2) | 3.9 | 10-29 | 3 | N |
| **This** | 725 | 90 (12.4) | 3.2 | 6.8-62.1 | 4 | Y |

IS – in-band isolation, CMS – in-band common-mode suppression, *N* – number of transmission poles, Bal. – balanced.

reciprocal filters in Table I. To the best of the authors' knowledge, this is the first and only non-reciprocal balanced BPF to be presented. Compared to the other non-reciprocal filters, the one presented here contains the greatest number of poles and obtains the highest in-band IS.

## IV. CONCLUSION

This manuscript reported on the design and implementation of a new type of a balanced BPF with a non-reciprocal and quasi-elliptic transfer function. Non-reciprocity is obtained through the STM of the resonant frequencies of some of the filter's resonators. The result is a quasi-elliptic bandpass response in the forward direction of propagation and highly-attenuated response in the reverse direction. The filter exhibits high levels of common-mode suppression through TZs and resistive loss that are unique to the common mode. For experimental validation, a microstrip prototype was designed, manufactured, and measured. It exhibits a reverse transmission IS of up to 62.1 dB while maintaining a low IL of 3.2 dB in the forward direction. It demonstrates a common mode suppression of up to 62 dB and at least 45 dB in over an octave of BW.

## REFERENCES

[1] W. Feng, W. Che and Q. Xue, "The proper balance: overview of microstrip wideband balance circuits with wideband common mode suppression," *IEEE Microw. Mag.*, vol. 16, no. 5, pp. 55-68, June 2015.

[2] R. Gómez-García, J. Muñoz-Ferreras, W. Feng and D. Psychogiou, "Balanced symmetrical quasi-reflectionless single-and dual-band bandpass planar filters," *IEEE Microw. Wirel. Compon. Lett.*, vol. 28, no. 9, pp. 798-800, Sept. 2018.

[3] D. Simpson and D. Psychogiou, "High-order and tunable balanced bandpass filters using mixed technology resonators," *Intern. Jour. Microw. Wirel. Tech.*, vol. 13, no. 7, pp. 673–681, 2021.

[4] H. -W. Deng, L. Sun, F. Liu, Y. -F. Xue and T. Xu, "Compact tunable balanced bandpass filter with constant bandwidth based on magnetically coupled resonators," *IEEE Microw. Wirel. Compon. Lett.*, vol. 29, no. 4, pp. 264-266, April 2019.

[5] Y. Zhang, Y. Wu, W. Wang and J. Yan, "High-performance common- and differential-mode reflectionless balanced band-pass filter using coupled ring resonator," *IEEE Trans. Circ. Syst. II: Express Briefs*, vol. 69, no. 3, pp. 974-978, Mar. 2022.

[6] W. Feng, B. Pan, H. Zhu, X. Y. Zhou, W. Che and Q. Xue, "High performance balanced bandpass filters with wideband common mode suppression," *IEEE Trans. Circ. Syst. II: Express Briefs*, vol. 68, no. 6, pp. 1897-1901, June 2021.

[7] Z. Zhang, G. Zhang, Z. Liu, W. Tang and J. Yang, "Compact balanced bandpass filter based on equilateral triangular patch resonator," *IEEE Trans. Circ. Syst. II: Express Briefs*, vol. 69, no. 1, pp. 90-93, Jan. 2022.

[8] Q. Liu, J. Wang, G. Zhang, L. Zhu and W. Wu, "A new design approach for balanced bandpass filters on right-angled isosceles triangular patch resonator," *IEEE Microw. Wirel. Compon. Lett.*, vol. 29, no. 1, pp. 5-7, Jan. 2019.

[9] W. Feng, W. Che and Q. Xue, "Novel wideband balanced bandpass filter based on multi-mode resonator," *42nd European Microw. Conf. (EuMC)*, 2012, pp. 392-395.

[10] X. Wu, M. Nafe, A. A. Melcón, J. Sebastián Gómez-Díaz and X. Liu, "A non-reciprocal microstrip bandpass filter based on spatio-temporal modulation," 2019 *IEEE MTT-S Intern. Microw. Symp. (IMS)*, 2019, pp. 9-12.

[11] X. Wu, X. Liu, M. D. Hickle, D. Peroulis, J. S. Gómez-Díaz and A. Álvarez Melcón, "Isolating bandpass filters using time-modulated resonators," *IEEE Trans. Microw. Theory Techn.*, vol. 67, no. 6, pp. 2331-2345, June 2019.

[12] D. Simpson and D. Psychogiou, "Magnet-less non-reciprocal bandpass filters with tunable center frequency," *49th European Microw. Conf. (EuMC)*, 2019, pp. 460-463.

[13] D. Simpson and D. Psychogiou, "Fully-reconfigurable non-reciprocal bandpass filters," *2020 IEEE MTT-S Intern. Microw. Symp. (IMS)*, 2020, pp. 807-810.

[14] X. Wu, M. Nafe, A. Á. Melcón, J. S. Gómez-Díaz and X. Liu, "Frequency tunable non-reciprocal bandpass filter using time-modulated microstrip λg/2 resonators," *IEEE Trans. Circ. Syst. II: Express Briefs*, vol. 68, no. 2, pp. 667-671, Feb. 2021.

[15] R. Gómez-García, J. Muñoz-Ferreras and D. Psychogiou, "Fully-reconfigurable bandpass filter with static couplings and intrinsic-switching capabilities," *2017 IEEE MTT-S Intern. Microw. Symp. (IMS)*, 2017, pp. 914-917.

[16] (2022) Skyworks SMV1413 product details. [Online]. Available: https://www.skyworksinc.com/Products/Diodes/SMV1413-Series